

A C/MoS₂ mixed-layer phase (MoSC) occurring in metalliferous black shales from southern China, and new data on jordisite

LI-SHUN KAO,^{*1} DONALD R. PEACOR,¹ RAYMOND M. COVENEY JR.,² GENGMEI ZHAO,¹ KEENAN E. DUNGEY,³ M. DAVID CURTIS,³ AND JAMES E. PENNER-HAHN³

¹Department of Geological Sciences, University of Michigan, Ann Arbor, Michigan 48109-1063, U.S.A.

²Department of Geosciences, University of Missouri, Kansas City, Missouri 64110-2499, U.S.A.

³Department of Chemistry, University of Michigan, Ann Arbor, Michigan 48109-1055, U.S.A.

ABSTRACT

A new phase composed mainly of Mo, S, and C and referred to herein as MoSC occurs widely in organic-rich, metalliferous Cambrian black shales in south China. MoSC, which has previously been referred to as jordisite, has been studied by scanning electron microscopy (SEM), electron microprobe analysis (EMPA), transmission electron microscopy (TEM), powder X-ray diffraction, (XRD), extended X-ray absorption fine structure (EXAFS), and catalytic activity. TEM data show MoSC to have a layered structure, with packets resembling molybdenite and graphite-like carbon that average five layers in thickness. Analytical data are consistent with an idealized formula of $\text{Mo}_3\text{S}_6\text{C}_{10}$ but it commonly contains 1–3 wt% each of Fe, Ni, and As so that its composition may be better approximated by the formula $(\text{Mo}, \text{Fe}, \text{Ni})_3(\text{S}, \text{As})_6\text{C}_{10}$. Selected area electron diffraction (SAED) patterns show a small number of broad, inhomogeneous rings corresponding to randomly oriented layers arranged in subspherical cells. A single broad, weak peak corresponds to a 10–11 Å layer spacing in powder XRD diffraction patterns. Pseudomorphism after fossil bacteria implies an origin by replacement of sedimentary organic material. In its chemical properties and structure, MoSC resembles synthetic compounds used as catalysts for hydrodesulfurization (HDS) in the petrochemical industry. The large surface-to-volume ratio for MoSC may be an important factor in its relatively strong HDS catalytic activity.

Cotype samples of jordisite from Germany, previously thought to be amorphous MoS₂, were also studied by SEM and TEM. Jordisite occurs as sequences of a few curved layers that form subspherical units, with an appearance remarkably like that of MoSC. However, the layer spacing is ~6 Å, like that of molybdenite. The ratio of Mo:S is ~1:2, and no carbon was detected, although it coexists with kerogen. Jordisite is thus confirmed to be a form of MoS₂, but because powder diffraction-like SAED patterns were obtained, it is not amorphous.

INTRODUCTION

Black shales are organic-rich rocks that commonly are enriched in metallic elements localized in specific horizons, as in the Permian Kupferschiefer of northern Europe. Some black shales contain economically significant concentrations of metals such as Cu, Co, Ni, Pb, Zn, U, and Mo. Numerous studies have shown that organic matter or sulfide minerals play important roles in concentrating metals, including Mo, from aqueous solutions. For example, either peat or algal remains can readily scavenge Mo (Szilagyi 1967; Bertine 1972; Disnar 1981). The association of Mo with organic matter was further demonstrated through the leaching of significant fractions of the Mo contained in the organic component of euxinic sediments by solvents consisting of alkanes (Nissenbaum and Swaine 1976) or other organic solvents (Volkov and Fomina 1974). The correlation between Mo and sulfide-S has been noted by Glikson et al. (1985) and Brumsack (1989), suggesting that sulfide ion is also a significant agent for fixation of Mo. Bertine

(1972) reported that the most effective scavenging mechanism is coprecipitation with Fe sulfide. Coveney and Glascock (1989) found that the Mo in the Mecca Quarry Shale of Indiana was associated with the surface of framboidal pyrite.

Despite the known association between Mo and black shales that are rich in organic matter and metallic sulfides, little is known about the structure and composition of the phases that contain the majority of the Mo. This is caused in part by the difficulty in characterizing fine-grained sediments. Nevertheless, Helz et al. (1996) attempted to characterize the local environment of Mo occurring in organic matter from a variety of black shales, including the Mecca Quarry Shale, using EXAFS spectra. They showed that Mo occurs in at least three different forms characterized by Mo-O, Mo-S-Fe, and Mo-S bonds. The Mo-S-Fe compound was theorized to have a cubane-type structure where Mo and S atoms occupy alternate vertices of a distorted cube. Helz et al. proposed that the Mo originated as MoO_4^{2-} in seawater, maturing through cubane-like forms and, ultimately, developing into a material resembling molybdenite. Nevertheless, the specific mineral in which Mo occurs was not characterized.

* E-mail address: kaols@umich.edu

Although molybdenite is by far the most common Mo-sulfide mineral, the ill-defined mineral jordisite has been reported from numerous locations. The name jordisite was proposed by Cornu (1909) for a black, powdery, colloidal, Mo sulfide that he believed to be amorphous and for which the Mo:S ratio is 1:2. Staples (1951) subsequently obtained the first chemical and X-ray data for similar material from Oregon, which he reported to be amorphous to X-radiation. Molybdenum occurs in high concentrations in black shale from south China (Chen et al. 1982; Fan 1983; Coveney and Chen 1991; Coveney et al. 1992). However, previous XRD analysis and ore microscopy of bulk ore samples containing 4–18% Mo failed to indicate the presence of any known Mo mineral except for the trace amounts of molybdenite reported by Fan (1983). Nevertheless, EMP analyses of ore samples were consistent with a Mo:S ratio of approximately 1:2. The Mo was therefore assumed to be present as jordisite (Fan 1983; Coveney et al. 1992).

As part of a comprehensive study of Chinese black shales rich in metallic elements, R. M. Coveney Jr. and associates collected samples of the Mo-rich black shales from Guizhou during 1988 and 1991. The present work involves the use of TEM and other methods to determine the nature of the principal Mo phase or phases present in these shales.

GEOLOGICAL SETTING

Unusual bedded Ni- and Mo-rich ore deposits, with cutoff grades near 4.5% Mo and with reported grades as high as 18.3%, occur as thin lenses in middle Cambrian black shales in south China (Chen et al. 1982; Fan 1983; Coveney and Chen 1991; Coveney et al. 1992). The metalliferous shales and their Ni-Mo deposits can be traced across a broad region of China, mainly south of the Yangtze River, in a belt of provinces extending from Yunnan on the west through portions of Guizhou, Sichuan, Hunan, and Jiangxi, to Zhejiang (Fig. 1). The Cambrian black shales that host the ore are approximately 60 to 150 m thick and include the Niutitang Formation of Guizhou and Hunan and stratigraphic equivalents elsewhere. The ore bed itself varies in thickness from a featheredge to ~30 cm and consists largely of pyrite, apatite, vaesite, MoSC, and gersdorffite (Fan 1983). The ore bed also contains quartz, carbonates and clay minerals, principally illite. Other thin beds with textures similar to those of the ores consist almost entirely of fluorapatite.

The four samples used for the present study were collected at Tianshan, Guizhou province near Zunyi. Three samples are from the sulfide-rich ore layer (Tess-1A, Tess-1C, and Tess-5) and contain in excess of 10–30% S and several percent each of Mo and Ni. The ore minerals occur in the form of oncrites arranged as an unusual polymictic conglomerate that probably formed near hydrothermal vents in the sea floor (Murowchick et al. 1994; Lott et al. 1999). The fourth sample consists of the host black shale (Tess-1B) that contains lesser amounts of sulfide minerals and only a few tenths of one percent heavy metals.

ANALYTICAL TECHNIQUES

Thin sections backed with sticky-wax (thermosensitive cement) were prepared for TEM studies. Other epoxy-backed thin sections were utilized for optical microscopy and scanning elec-

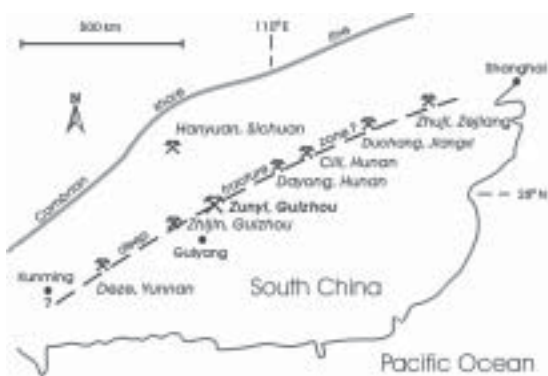


FIGURE 1. Map of Guizhou and Hunan provinces, southern China (Coveney and Chen 1991), showing the locations of mines that provided samples of the sulfide-rich layers.

tron microscopy (SEM) using a Hitachi S3200 instrument fitted with backscattered electron (BSE) detectors and a Noran EDS analytical system. Samples with and without C-coatings were used in order to permit analysis of C-rich areas of the samples. The EMPA were carried out with a Cameca CAMEBAX instrument operated at 20 kV and a beam current of 9.8 nA. Both natural and synthetic mineral standards were used, with corrections carried out with the PAP method. Carbon analyses with the EMPA were carried out using synthetic metal-C compounds as standards. TEM samples were prepared by attaching Al washers to selected areas of sticky-wax backed thin sections that were selected on the basis of optical and SEM study. The selected samples were ion-milled and C-coated for study with a Philips CM12 TEM equipped with a Kevex Quantum EDS detector system, and operated at 120 kV. Point-to-point resolution is ~3.4 Å and line-to-line resolution is ~2.0 Å. AEM quantitative chemical analyses were obtained in scanning mode with an electron beam approximately 50 Å in diameter and processed using the procedures described by Lorimer and Cliff (1976). The relative 2s error (from counting statistics) for major elements (oxides >10 wt%) is 2–5% and for minor elements (oxides 1–10 wt%) is 5–10%. Special procedures were taken in order to separate the overlapping SK α and MoL α peaks. First, the ratio of MoL α to MoK α was obtained from Mo metal. This ratio and the intensity of the MoK α peak were used to compute the intensity of MoL α , which was subtracted from the intensity of the overlapping SK α and MoL α peaks. Application of the method to standards resulted in accurate element ratios.

When it was recognized that MoSC is analogous to synthetic compounds that are models for catalysts in desulfurization of organic compounds (Dungey et al. 1998a), we tested the catalytic hydrodesulfurization (HDS) activity of the new phase. Attempts to extract the organic component by refluxing and sonicating in CDCl₃, benzene-d₆, or toluene-d₈, failed, so that the HDS measurements were obtained using powdered bulk-shale samples. A 0.623 g sample of Tess-5 was loaded into a fixed-bed microreactor and its catalytic activity toward the HDS of thiophene was determined in a thiophene/hydro-

gen stream with a flow rate of 10 mL/min, using a procedure analogous to that described previously for synthetic catalysts (Dungey et al. 1998a). Three measurements were taken on the same sample: untreated Tess-5; reduced at 400 °C in a 20 mL/min flow of H₂ for 4 h (Tess-5R); and reduced for a second time (Tess-5R2). After the measurements were taken, the reactor was sealed and the remaining material recovered in a dry box, yielding 0.515 g of black powder (17% weight loss). Portions were later analyzed by X-ray absorption spectroscopy. Surface area was determined to be 15.4 m²/g by single-point Brunauer-Emmett-Teller (BET) analysis of samples degassed in H₂ for 3 h at 400 °C. The HDS activity of powdered 2H-MoS₂ (Strem Chemical Co.) was studied under the same conditions (untreated MoS₂, and reduced MoS₂R). For comparison with a conventional HDS catalyst, an alumina supported, Co-promoted catalyst (CoMo/A) was prepared from commercially available pre-loaded material (14.0% MoO₃, 3.5% CoO on Al₂O₃, Strem Chemical Co.) by diluting to 1% metal with alumina and pre-sulfided on-line in a 10% stream of H₂ containing 10% H₂S (10 mL/min, 400 °C, 4 h).

X-ray absorption spectra were measured at 10K at the Stanford Synchrotron Radiation Laboratory (SSRL) on beam line II-3, with synchrotron energies of 3.0 GeV and a stored current of 100 mA. For each sample, the absorption spectrum of Mo foil was monitored to standardize the energy scale, with the first inflection point of Mo defined as 20000.0 eV. Spectra were recorded from 19700 eV to 21200 eV, with a k_{\max} value of 17 Å⁻¹. Other experimental details were as described for synthetic MoS₂ intercalation compounds (Dungey et al. 1998b), and data were analyzed according to established methods (Teo 1986).

XRD measurements were carried out on an oriented MoSC thin section with a Scintag X₁ advanced diffraction system at 35 kV and 20 mA, utilizing CuK α radiation and a Peltier-cooled solid-state X-ray detector.

RESULTS

SEM observations

BSE images (Fig. 2) of the sulfide-poor black shale (Tess-1B), show that it has a texture typical of pelitic sediments in that it consists of detrital quartz, K-feldspar, albite, muscovite, and chlorite coexisting with authigenic apatite, sphalerite, and pyrite. Organic material occurs as domains less than 1 mm in size elongated parallel to bedding. EDS analyses indicate small but uniform contents of S and V. The matrix consists largely of illite, for which EDS spectra consistently show a small amount of V. Similar V-rich illite has been described from the Mecca Quarry Formation at Velpen, Indiana (Peacor et al. 2000). The upper part of Figure 3 shows pyrite-rich material with a texture that is typical of the 10 to 30 cm sulfide-rich layer. The MoSC phase occurs with two different textures. As can be seen at the lower part of Figure 3, MoSC occurs as more-or-less continuous lenses interstitial to angular grains of quartz, apatite, and V-rich illite. In contrast, some MoSC occurs as rounded grains (Fig. 4) that form discontinuous layers ~1 mm thick. The fractures, which are shown in Figure 4, may be shrinkage cracks. Both types of MoSC, as well as associated grains of apatite, are fractured and veined with quartz and barite. Qualitative EDS analyses of MoSC show that it has Mo:S ~ 1:2, major

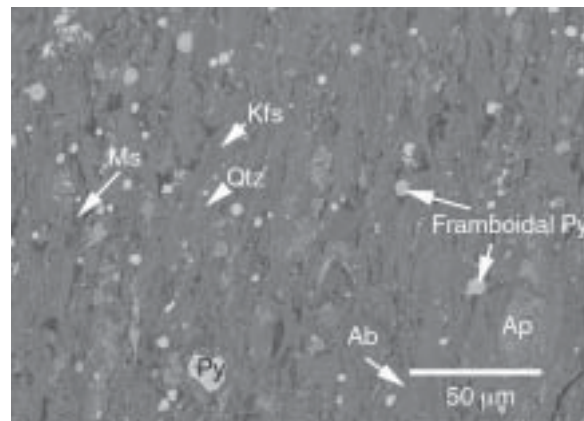


FIGURE 2. Backscattered electron (BSE) image of a MoSC-free area with pyrite (some of which is frambooidal), apatite, V-rich illite, quartz, and albite. (Py = pyrite; Ap = apatite; Ab = albite; Qtz = quartz.)

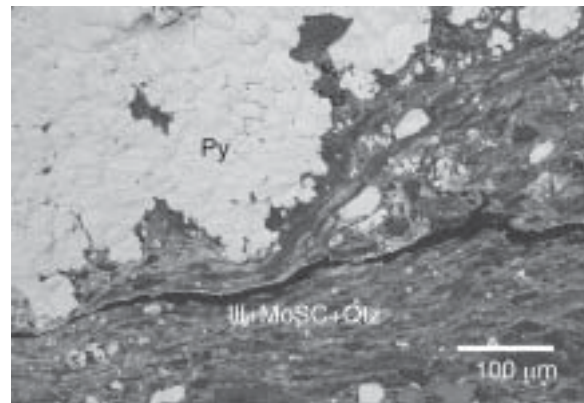


FIGURE 3. BSE image of an ion-milled sample showing pyrite nodules and MoSC associated with V-rich illite.

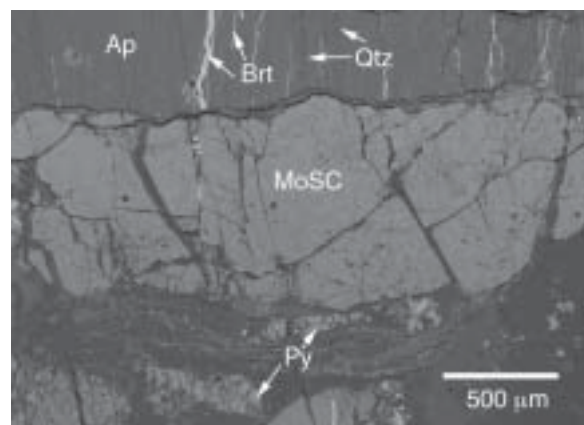


FIGURE 4. BSE image of MoSC nodules. Sulfides and clay minerals occur within the nodules. (Py = pyrite; Ap = apatite; Brt = barite; Qtz = quartz.)

amounts of C, minor amounts of Fe and Ni, and minor As in some areas.

TEM observations

Figure 5 is a lattice-fringe image that was obtained using the diffraction pattern shown in the inset. The diffraction pattern consists of continuous and diffuse rings that are uniform in contrast, implying that it is derived from very fine-grained material. The rings are extremely broad, probably because of variations in *d*-values. The largest *d*-value, which is provisionally labeled *d*(001), is 10–11 Å; other *d*-values correspond to 002, and 003 of MoSC (Table 1). The lattice-fringe image shows fringes for which most spacings are 10–11 Å, varying slightly along layer. The fringes are curved and commonly form hollow, ellipsoidal units. Such textures, which were observed only in two-dimensional views, are inferred to correspond to subspherical cells in three dimensions. They resemble textures of smectite found as an alteration product of volcanic glass (Masuda et al. 1996) and some artificial MoS₂ catalysts (Payen et al. 1989; Datye et al. 1996). Packets of layers may contain as few as two or three layers, but most are about five layers thick. Although the lattice-fringe images are dominated by fringes having spacings of average value ~10.3 Å, other spacings occur that have values of approximately 3, 6, 12–13, and 15–16 Å, in part accounting for the diffuseness of diffraction patterns (Fig. 6). AEM analyses of the areas showing such lattice fringes give a Mo:S ratio of 1:2, and indicate the presence of small amounts of Ni and Fe. AEM analyses of MoSC were regarded as qualitative insofar as the Mo:S ratio is concerned,

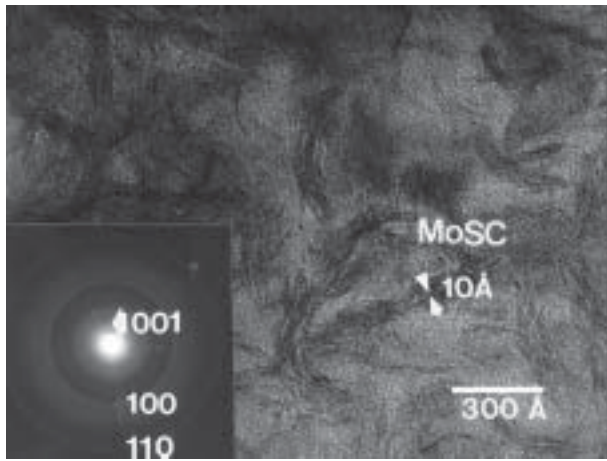


FIGURE 5. HRTEM image of MoSC showing curved layers that commonly form closed cells. Inset: SAED pattern with the form of a powder pattern.

TABLE 1. *d*-values for MoSC SAED powder patterns

<i>d</i> value(Å)	Intensity*
10.5	80
5.2	40
3.4	20
2.8†	100
1.6†	50

* Intensities visually estimated.

† *d*-value corresponds to pyrite and vaesite.

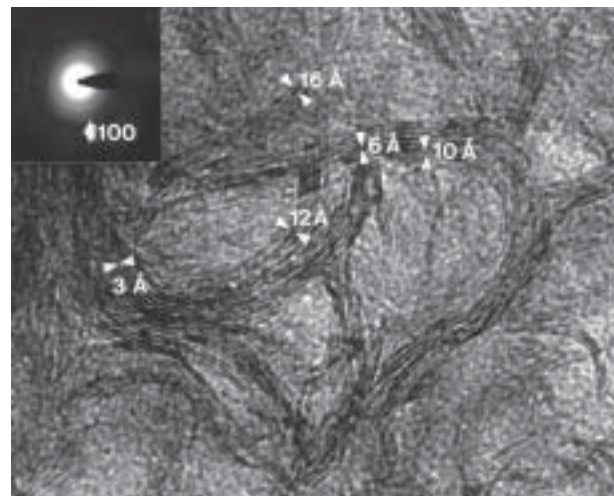


FIGURE 6. HRTEM image of MoSC showing lattice fringes with variable thickness. Inset: SAED pattern with the form of a powder pattern.

TABLE 2. Relative atomic proportions for selected AEM analyses of MoSC

	1	2	3
S	2	2	2
Fe	0.24	0.37	0.33
Ni	0.10	0.09	0.04
As	0.09	0.08	0.00
Mo	0.93	0.90	0.74

1,2 = area with many visible lattice fringes.

3 = area with few visible fringes.

because of the direct overlap of the SK α and MoL α peaks, the latter being the only relatively intense Mo peak (Table 2). A CK α peak with intensity on the order of 5% of the intensity of the combined Mo-S peak was observed. In order to determine the degree to which the sample's carbon coating could contribute to the CK α peak, analyses were obtained from non-C containing minerals such as quartz. No C was detected. The CK α peak was therefore assumed to correspond to a significant C content in MoSC, but a quantitative measure of the concentration could not be obtained by AEM.

In order to obtain better definition of the diffraction relations, images were first obtained that showed layers that were continuous for hundreds of angstroms (Fig. 7). The diffraction pattern of such material (inset of Fig. 7) shows broad single-crystal-like reflections with inhomogeneous intensity, with *d*-values that are identical to those of ring patterns, but which are superimposed on diffuse arcs.

EMPA data

Analyses were obtained only for the MoSC that occurs as rounded grains in continuous layers, because such material occurs in relatively homogeneous grains that are much larger than the region of interaction of the electron beam of EMPA. Analyses gave a Mo:S ratio of 0.75:2 (Table 3). Interestingly, Fe, Ni, and As contents are similar in both quantitative analyses, implying that the presence of these metals may not be due

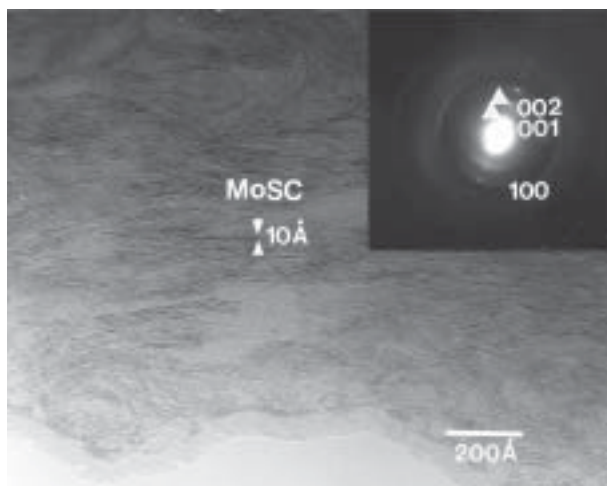


FIGURE 7. HRTEM image showing wavy, subparallel MoSC fringes. The inset SAED pattern has diffuse, periodic reflections, lying along a vector normal to the fringes.

TABLE 3. EMPA analyses of MoSC

wt%	1	2
S	26.1	25.48
Mo	29.2	29.14
V	0.49	0.47
Fe	2.89	2.58
Ni	2.82	2.86
As	1.91	2.16
Se	0.58	0.66
C*	36.56	36.40
Total	100.55	99.75
Atomic proportions*		
S	2.00	2.00
Mo	0.75	0.76
V	0.02	0.02
Fe	0.13	0.12
Ni	0.12	0.12
As	0.06	0.07
Se	0.02	0.02
C†	7.48	7.63

* Obtained by difference.

† Normalized to 2 S atoms.

to contamination by other phases, but that they are essential constituents of MoSC. (It should be noted, however, that qualitative AEM analysis of samples showed considerably less Fe and Ni in one sample and no As). The EMP analyses are for relatively large millimeter-scale areas. Although such areas consist largely of MoSC, they also include some component of amorphous material that was observed by AEM to have less Mo relative to S than corresponds to the ratio 1:2.

Quantitative analyses for C were obtained using a crystal of PC-2, and metal-C standards for C. All carbon analyses were carried out with no C coatings on the samples. EMP analyses were only semi-quantitative due to uncertainties in the C-content of the standards, but values were obtained that ranged from 35 to 50% with various standards. Because the values of concentrations for other elements were inferred to be accurate, the value for C (~36 wt%) was obtained by difference (Table 3). The larger values obtained for C from some EMP analyses were

inferred to be consistent with the maximum, but smaller, value as calculated by difference, given the relatively large errors in direct analyses of C.

X-ray absorption spectra

The data described above imply that MoSC has a Mo:S ratio of approximately 1:2, similar to that of molybdenite, and that it has a layered structure that provides a further analogy to that mineral. In order to obtain more definitive data, the coordination environment and oxidation state of Mo in sample Tess-5 was obtained from MoK edge X-ray absorption spectra. The EXAFS data can be fit to three shells of scattering atoms (Fig. 8 and Table 4). The first coordination shell consists of S atoms at a distance corresponding to a Mo-S single bond (2.40 Å). The second shell was fit to 3.5 Mo atoms at a distance of

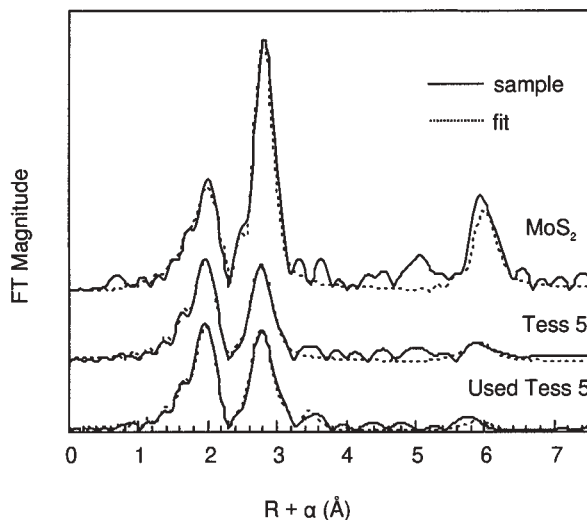


FIGURE 8. Fourier-transformed (FT) Mo EXAFS spectrum of pure 2H-MoS₂ (MoS₂) sample Tess-5 before (Tess-5) and after HDS-processing (Used Tess-5).

TABLE 4. Fitting parameters for Mo EXAFS of Tess-5

Sample	Tess-5	Used Tess-5	2H-MoS ₂
S1	CN	5	6
	R	2.40	2.42
	σ ²	2.5	2.8
Mo1	CN	3.5	6
	R	3.15	3.16
	σ ²	2.5	1.6
S2	CN	2	
	R	3.98	
	σ ²	0.4	
Mo2	CN	2	3
	R	6.38	6.40
	σ ²	3.8	0.9
F	0.036	0.038	0.051

Note: CN is the number of scatterers, R is the absorber-scatterer distance in Å, σ² is the Debye-Waller factor in Å² × 10³ for each shell. F = $(\sum(\chi_{\text{obs}} - \chi_{\text{calc}})^2 / [N_{\text{pts}} \cdot N_{\text{var}}])^{0.5}$ goodness of fit index. The threshold energy (E₀) for all shells in all fits was 24.0 eV, whereas the scale factor was set to 1.1.

3.15 Å. The third shell corresponds to longer in-plane Mo-Mo interactions (6.38 Å). These data are consistent with equivalent parameters of molybdenite, although all three shells have smaller coordination numbers than would be expected for molybdenite. This could be caused by the small particle size and/or by disorder that is observed in TEM images.

The X-ray absorption near-edge structure (XANES) of Tess-5 is slightly shifted to higher energy (2.5 eV) than the absorption edge of 2H-MoS₂ (Fig. 9). A shift to higher energy usually indicates an increase in oxidation state, although the coordination geometry will also affect the XANES (George et al. 1989). The absence of a pre-edge feature suggests that there are no Mo = O or Mo = S double bonds present (which give rise to 1 $s \rightarrow 4d$ transitions) (Leliveld et al. 1997). Therefore the sample does not contain the Mo (IV) species MoO₄²⁻ and MoS₄²⁻. As X-ray absorption spectra are average signals from the bulk sample, the differences between Tess-5 and MoS₂ may be due to the averaging of MoS₂ with a minor amount of a Mo phase containing Mo-S single bonds and a higher oxidation state than Mo (IV). The X-ray absorption data indicate that the dominant Mo-containing phase has a local structure resembling that of molybdenite.

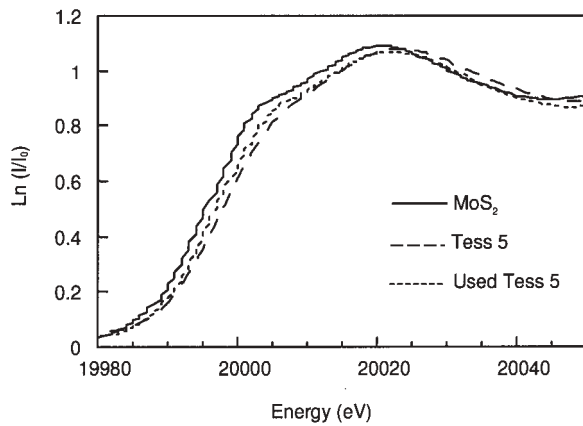


FIGURE 9. XANES spectrum of pure 2H-MoS₂, and the MoSC sample Tess-5, before and after HDS processing. $\ln(I/I_0)$ = natural logarithm of relative intensity.

TABLE 5. HDS of thiophene by Tess-5 catalysts in 1 atm of H₂ (10 mL/min*)

Catalyst	T (K)	Rxn rate†	propene	i-butane	i-butene	butane	1-butene	c-butene	t-b utene	butadiene
TESS5	543	6.4	231	0	523	148	393	529	891	45
mol%			8	0	19	5	14	19	32	2
MoS ₂	543	2.1	179	0	0	47	123	112	105	36
mol%			30	0	0	8	20	18	17	6
TESS5R	573	8.5	472	39	1250	243	488	470	722	0
mol%			13	1	34	7	13	13	20	0
TESS5R2	573	9.2	518	47	1334	245	550	521	770	0
mol%			13	1	33	6	14	13	19	0
MoS ₂ R	573	5.3	156	3	89	122	677	355	406	109
mol%			8	0	5	6	35	19	21	6
CoMo/A	573	39	249	0	149	313	1780	2609	4174	85
Mol%			3	0	2	3	19	27	44	1

* All reaction products are reported in pmol.

† The rate of reaction is expressed as nmol products/g cat. •s.

HDS catalytic activity

For over 50 years, the petroleum industry has used CoMoS and NiMoS materials to remove S from crude oils by catalytic hydrodesulfurization (HDS). The conventional catalyst is ideally composed of a monolayer of molybdenite on alumina, with Co or Ni salts added to promote the catalytic activity. This complex, amorphous material has been difficult to characterize and there has been much speculation about the structure and role of the various components (Chianelli et al. 1994; Topsøe et al. 1996). One model for the active site in CoMoS catalysts is pseudo-intercalation, in which Co (II) ions coordinate to the edge of the molybdenite-like MoS₂ layers (Farragher and Cossee 1972). This model was recently tested through the synthesis of intercalation compounds of MoS₂ (Brenner et al. 1998; Dungey et al. 1998a). Because the data on MoSC were consistent with a Mo:S ratio and layered structure that appeared to be closely related to such compounds, and because the TEM data showed that MoSC has a high surface area structure as required of catalysts, we tested sample Tess-5 for catalytic activity toward the HDS of thiophene (Table 5).

There are a variety of ways of evaluating the catalytic activity for a heterogeneous reaction. The rate of reaction reported in Table 5 is based upon the amount of product produced per mass of catalyst per time. In this comparison, untreated MoSC has a catalytic activity more than twice that of untreated molybdenite (6.4 vs. 2.1 nmol/gs). Re-activation of used HDS catalysts is done routinely by reducing or sulfiding. We simulated this on-line by reducing the used Tess-5 sample in a hydrogen stream at elevated temperatures. After reduction, catalytic activity increased (8.5 nmol/gs), outperforming reduced molybdenite (5.3 nmol/gs). Further reduction did not significantly increase the activity of Tess-5. Although the activity is greater than that of MoS₂, it is less than that of a synthetic intercalated MoS₂-organometallic compound [14.3 nmol/gs for $[(C_3H_5)_2Co]_{0.14}MoS_2$ (Dungey et al. 1998a)], and is only about 25% as active as a conventional, alumina supported catalyst (39 nmol/gs for CoMo/A).

The above results do not establish the number or quality of active sites present on the surface of the catalyst. For example, the alumina-supported catalyst, CoMo/A, has a small amount of metal, which is spread out as a monolayer over the alumina (Stockmann et al. 1995). Although determining the exact number of active sites can be difficult, the number of active sites is generally proportional to the surface area of the active mate-

rial. The measured surface area of the ore sample was 15.4 m²/g whereas that of the 2H-molybdenite sample was 6 m²/g. The respective activities per area, therefore, were substantially the same at 0.60 and 0.88 nmol/m² s. The cause of the enhanced activity of MoSC is therefore attributed to the greater surface area per mass, which is consistent with the structures observed by TEM.

The Tess-5 catalyst samples gave 19–34% i-butene and 8–13% propene in the product slots. These rearrangement and hydrogeneolysis products are always formed to some extent in HDS of thiophene and are usually attributed to the presence of acidic sites on the catalyst surface (Topsøe et al. 1996).

Catalytic materials often change during use. For example, a dramatic de-intercalation is observed for synthetic mixed-layer MoS₂ materials after use as HDS catalysts (Dungey et al. 1998a). Therefore we collected X-ray absorption data for the used Tess-5 sample in order to obtain structural information. XANES spectra (Fig. 9) and EXAFS spectra (Fig. 8, Table 4) are very similar to that of the fresh Tess-5 sample. Unlike the changes observed in synthetic intercalation catalysts, the MoSC is stable under the HDS reaction conditions. Unfortunately, the Mo K edge XAS does not give any information about the presence or absence of intercalant, and so the fate of the C-containing interlayer in MoSC (see below) is unknown.

X-ray diffraction

XRD data were obtained for a thin section for which SEM data had indicated a relatively large proportion of MoSC and only traces of illite. The thin section was oriented normal to sedimentary layering, so that the illite, which has *d*(001) close to that of MoSC, could not contribute significantly to the diffraction pattern. There is a weak, diffuse peak at 8.75 °2θ, for which the *d*-value is 10.11 Å (Fig. 10), which corresponds to that obtained by electron diffraction for MoSC. Because of the extreme breadth of the reflection, as consistent with SAED patterns of MoSC but not with illite, the reflection is inferred to be due to MoSC.

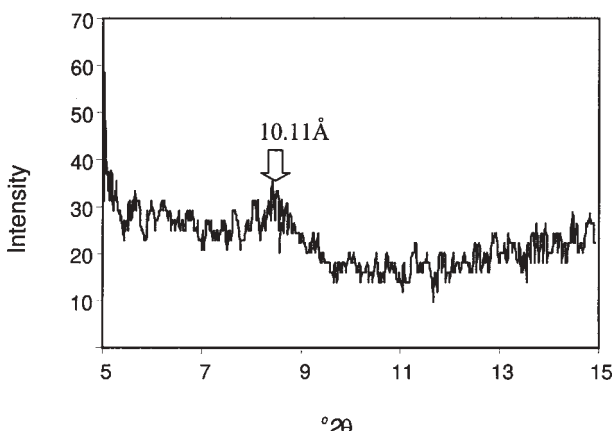


FIGURE 10. Part of the XRD pattern of a thin section of MoSC-containing sample, sectioned perpendicular to the bedding plane.

Data for jordisite

Because the data for MoSC implied a close relationship to jordisite, we obtained a cotype specimen of jordisite. Samples were observed by SEM and TEM. As shown by Figure 11, the jordisite occurs in our sample as irregular veins bordering quartz and apatite. The lattice-fringe images (Fig. 12) are strikingly similar to those of MoSC in that they consist of thin packets with curved fringes that commonly form hollow units with ellipsoidal shapes. Contrary to reports that it is X-ray amorphous, a powder-diffraction-like SAED pattern was obtained (inset, Fig. 12). The *d*-value of the principal line is 6.1 Å, and the corresponding interplanar spacing of lattice fringes is ~6 Å, a value that corresponds to the spacing of the layers of molybdenite. Some jordisite is bordered by organic material (Fig. 13), suggesting a further analogy with MoSC. Although AEM analyses of the organic material gave rise to relatively intense C peaks, but without peaks due to S or Mo, no carbon was detected in analyses of jordisite, seeming to confirm that it is MoS₂ in composition.

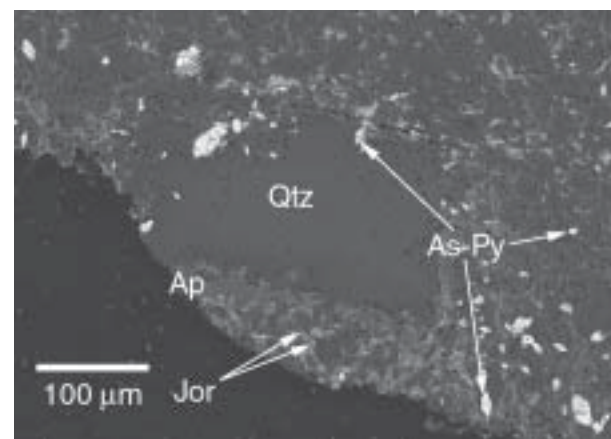


FIGURE 11. BSE image of a thin section showing jordisite coating the surface of quartz. The dark material on the lower left is epoxy. (As-py: arsenic-bearing pyrite.)

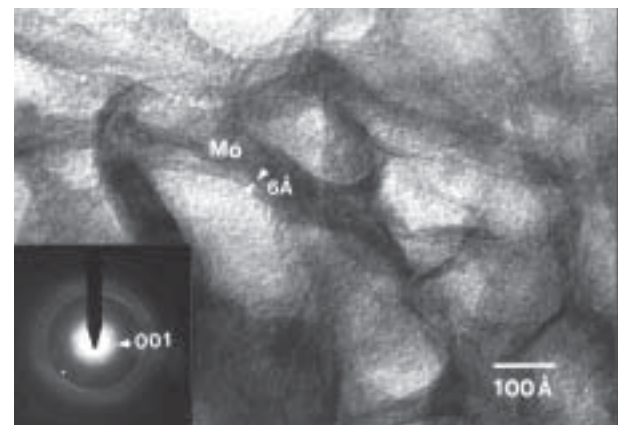


FIGURE 12. HRTEM image and SAED pattern of jordisite. Curved lattice fringes resemble those of MoSC, but have a spacing of ~6 Å, which corresponds to the spacing of molybdenite layers.

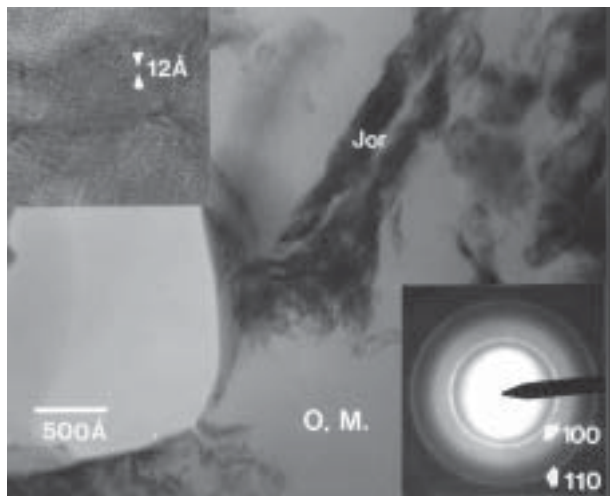


FIGURE 13. BF image of jordisite associated with kerogen. The inset SAED pattern shows only a diffuse ring pattern. Curved lattice fringes in the inset HRTEM image resemble those of MoSC, but have a spacing of $\sim 12 \text{ \AA}$, twice that of the spacing of molybdenite layers.

DISCUSSION

Composition and structure

The EMP analytical data indicate that MoSC from Tianmenshan, China has an idealized composition of MoS₂C₈. The Mo-edge XANES and EXAFS data support a molybdenite-like local structure and oxidation state for MoSC. The SAED patterns and lattice-fringe images imply that the structure is layered. This conclusion is supported by analogy with the plethora of synthetic compounds that are used as catalysts in the desulfurization of petroleum. HRTEM studies of conventional, alumina-supported HDS catalysts (Chianelli et al. 1995) and synthetic intercalation compounds of MoS₂ (Brenner et al. 1998) demonstrate the distorted morphology of the MoS₂ layers, similar to the curved structures observed in the MoSC. MoSC is a remarkable catalytic natural material with properties rivaling those of synthetic mixed-layered catalysts. Although its normalized HDS activity is only about half that of a Co-intercalated synthetic material (0.60 vs. 1.27 nmol/m² s for [(C₅H₅)₂Co]_{0.14}MoS₂), it must be noted that Co is a known promoter of HDS activity and that no Co has been added to MoSC either naturally or for our experiments. Up to 4% Ni, which can also be a promoter (Datye et al. 1996), is naturally present in the Chinese ores although much of it is present in vaesite (NiS₂) and gerdosoffite (NiAsS). The amount of Ni in the MoSC is comparable with, but smaller than, the amount of Co in [(C₅H₅)₂Co]_{0.14}MoS₂ (4.35 wt% Co).

A recent discussion has focused on the role of carbon in HDS catalysts, which may be incorporated into the catalyst from the petroleum feedstock (Chianelli and Berhault 1999). Molybdenum sulfide catalysts supported on carbon exhibit substantially increased HDS catalytic activity in comparison with material where alumina is used as the support (Vissers et al. 1987). An EXAFS study of the carbon-supported material indicated the presence of C in the coordination shell of Mo and it

has been proposed that C is a promoter of catalysis (Bouwens et al. 1990). MoSC from China is a naturally occurring intercalation compound of carbon in MoS₂ (see below), presenting a unique opportunity to further explore the role of carbon in promoting HDS catalysis.

Although lattice-fringe images of MoSC show curved fringes with spacings that are variable in the range 10–11 \AA , fringes of other spacings were occasionally observed intercalated with those of normal spacing. Those fringes have spacings of ~ 3 , 6, 12–13, and 15–16 \AA . The structures of graphite and molybdenite are layered, with fundamental layers having thickness of ~ 3.36 and 6.15 \AA , respectively (e.g., Gaines et al. 1997). The analogy with the observed fringe spacings suggests that graphite and molybdenite layers may constitute the basic building blocks of the MoSC structure with larger fringes corresponding to different proportions of the unit layers. Thus, the common fringes with spacings of 10–11 \AA would correspond to a combination of one graphite-like and one molybdenite-like layer. This structural analogy is further supported by the lattice spacings observed in synthetic polycyclic aromatic hydrocarbon (PAH) intercalation compounds of MoS₂. A 1,10-phenanthroline material has a *c*-value of 9.7 \AA (Golub et al. 1996), a series of naphthalene compounds that exhibit an increase in interlayer spacing of 2.4–4.3 \AA (Kosidowski and Powell 1998). In both of these materials, it was proposed that the plane of the aromatic molecule was parallel to the MoS₂ layers. Thus MoSC, with a *c*-lattice parameter of 10–12 \AA , probably consists of intercalated planar aromatic species or graphite layers oriented parallel to MoS₂ sheets. The other spacings observed by TEM may indicate the occurrence of stacking of different relative proportions of the same layers.

Variations in the combinations of MoS₂ and graphitic layers would correspond to unique bulk compositions that should permit one to predict *d*-values (Table 6). For example, the combination of two graphite and one MoS₂ layers gives a C content of 33.1 wt%, in good agreement with the observed EMP value of 36.5 wt% for samples of MoS₂C₈ from China. The predicted spacing of such a layered structure ($\sim 13 \text{ \AA}$) exceeds that of the average fringe spacing (10–11 \AA), however. The lack of agreement between observed spacing, predicted structure, and observed C content is mitigated in part, however, by the known errors in EMP analysis that must be caused by the presence of the amorphous organic component associated with concentrations of MoSC layers.

The role of Fe and Ni in the composition and structure are ill-defined. This uncertainty suggests that they may be essential components of the mineral. The sum of Mo, Fe, and Ni, as shown by the EMP data, is almost exactly equal to 1, relative to 2 S, suggesting the unlikely possibility of solid solution of Fe and Ni for Mo. All qualitative EDS analyses are consistent with the EMP data of Table 3 in showing the presence of Fe and Ni in small, subequal amounts, homogeneously distributed.

TABLE 6. Data for MoS₂-carbon mixed-layer structures

Carbon wt%	No. of graphite layers	No. of molybdenite layers	Thickness (\AA)
19.8	1	1	10–11
33.1	2	1	12–13
42.6	3	1	15–16

In summary, the collective data imply that MoSC has a layered structure. MoSC contains major amounts of C (~3–4 C per 2 S), but additional elements such as H could be associated with the C. The Mo:S ratio is 1:2 or nearly so, and the structure has a component that resembles molybdenite. The data therefore imply that the structure is based on mixed-layering of C-based and molybdenite-like basic layers with an overall ideal composition of $\text{Mo}_3\text{S}_6\text{C}_{10}$ and an actual composition of $(\text{Mo},\text{Fe},\text{Ni})_3(\text{S},\text{As})_6\text{C}_{10}$. MoSC therefore appears to be a new mineral and worthy of a mineral name. No attempt has been made to apply for mineral status to the I.M.A. Commission on New Minerals and Mineral Names, however, as the precise composition and structure remain to be defined.

Origin of MoSC

Abundant fossils of microorganisms including bacteria have long been known to be associated with the Chinese ores (Fan 1983; Murowchick et al. 1994; Lott et al. 1999). As shown in Figure 14, TEM images of MoSC in some cases showed rather remarkable circular features. These features have contrast defined by variable density of MoSC. There is a closely spaced pair of circles defining the outer boundary, having diameters of approximately 0.3 mm. These features have a striking resemblance to bacterial structures, the two bounding circles possibly corresponding to the inner and outer cell walls. Paleontologists familiar with such features have observed these images and concluded that they have the appropriate size and form and do indeed correspond to cross-sections of bacteria (e.g., Fisher, pers. comm., 1999). Such data imply that MoSC originated through replacement of solid organic matter as inferred by Murowchick et al. (1994).

Detailed analysis of the clay minerals associated with the Chinese ores (Kao, in preparation) has shown that, although the Mo and other metallic elements owe their origins to interaction of marine fluids and sediments at or near the water-sediment interface (Murowchick et al. 1994), the present mineral assemblage owes its origin to a fluid-rock event that post-dates low-grade metamorphism. Such low-grade metamorphism within slightly buried sediments on the sea floor would be entirely consistent with the models of deposition of Murowchick et al. (1994) and Lott et al. (1999). Field data and fluid inclusion results indicate that the ores formed at temperatures up to 260 °C within a Cambrian hydrothermal submarine vent system (Lott et al. 1999). Sulfur isotope studies have demonstrated that the sulfur present in the ores was derived through bacterial reduction (Murowchick et al. 1994). Thus, these remarkable ores formed in a complex environment through processes that include biologic activity.

Jordisite

Since Cornu (1909) first used the term jordisite for powdery, colloidal Mo sulfide from a hydrothermal ore deposit at the Himmelsfurst mine, near Freiberg, Saxony, Germany, the mineral has been ill-defined. Jordisite was described as a precursor for ilsemannite ($\text{Mo}_3\text{O}_8 \cdot \text{H}_2\text{O}$) at the Himmelsfurst mine. The composition and structure were defined by Staples (1951) for material from the Kiggins mine in Oregon, USA. Staples (1951) separated jordisite from coexisting minerals with bro-

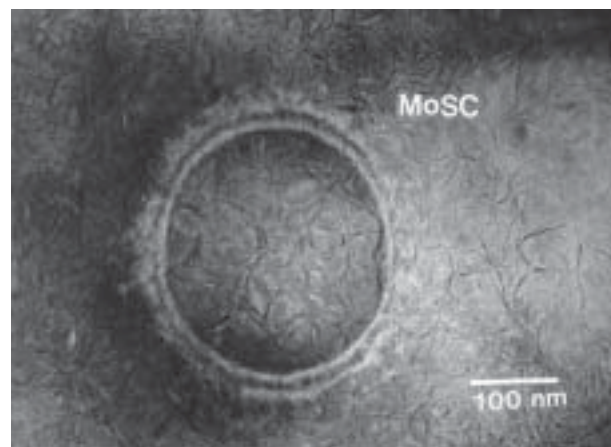


FIGURE 14. HRTEM image of a cross-section of a fossil bacterium that has been replaced by MoSC.

mofrom. Analysis of the separate gave 59.8 wt% Mo and 40.2 wt% S on a relative basis. The powder XRD pattern showed only quartz peaks, although Staples (1951) noted that Donnay observed some broad bands on all diffraction patterns that might have resulted from colloidal matter.

The data described above show that jordisite has a layered structure with layer spacing approximately equal to that of molybdenite (~6 Å), and a composition with Mo:S = 1:2 with no detectable carbon. Rather than being amorphous, however, it is crystalline in that SAED patterns have broad, powder-like diffraction rings, consistent with the observations of Donnay. These data indicate that jordisite is indeed poorly crystalline MoS₂, but with TEM images showing an unusual texture that is strikingly similar to that of MoSC. The coexistence of kerogen with jordisite also suggests a relation to MoSC, especially insofar as such kerogen is relatively unusual in hydrothermal veins. Nevertheless, the collective data show that jordisite and MoSC are distinctly different materials.

ACKNOWLEDGMENTS

The manuscript benefited greatly from reviews by Bertrand Devouard, James Brenner and Huifang Xu. We are grateful to D. Wolf, Prof. Herzig, and Karin Rank for making cotype samples of jordisite available for study, and to Carl Henderson for his help with the EMPA analyses, and to numerous past collaborators, most especially field companions, Anne M. Coveney, James B. Murowchick, UMKC, Richard I. Grauch, USGS, and Chen Nansheng, CAS. We thank L. Thompson, UM, for the use of the instruments in his laboratory for the BET measurements. D. Fisher of the Museum of Paleontology, University of Michigan, provided essential advice on the identity of the fossil bacteria. This research was supported in part by NSF grants EAR 94-18108 to DRP, EAR 89-17322 to RMC, and CHE-9523056 to MDC. K.E.D. is grateful to the College of Literature, Sciences and Arts, The University of Michigan, for a Regent's Fellowship.

REFERENCES CITED

- Bertine, K.K. (1972) The deposition of molybdenum in anoxic waters. *Marine Chemistry*, 1, 43–53.
- Bouwens, S.M.A.M., Prins, R., Beer, V.H.J.D., and Koningsberger, D.C. (1990) Structure of the molybdenum sulfide phase in carbon-supported Mo and Co-Mo sulfide catalysts as studied by extended X-ray absorption fine structure spectroscopy. *Journal of Physical Chemistry*, 94, 3711–3718.
- Brenner, J., Marshall, C.L., Ellis, L., Tomczyk, N., Heising, J., and Kanatzidis, M. (1998) Microstructural characterization of highly HDS-active Co_6S_8 -pillared molybdenum sulfides. *Chemistry of Materials*, 10, 1244–1257.

- Brumsack, H.J. (1989) Geochemistry of recent TOC-rich sediments from the Gulf of California. *Geologische Rundschau*, 78, 851–882.
- Chen, N., Yang, X., Liu, D., Xiao, X., Fan, D., and Wang, L. (1982) Lower Cambrian black argillaceous and arenaceous rock series in south China and its associated stratiform deposits. *Mineral Deposits*, 1, 39–51 (in Chinese).
- Chianelli, R.R. and Berhault, G. (1999) Symmetrical synergism and the role of carbon in transition sulfide materials. *Catalysis Today*, 53, 375–366.
- Chianelli, R.R., Daage, M., and Ledoux, M.J. (1994) Fundamental studies of transition-metal sulfide catalytic materials. *Advances in Catalysis*, 40, 177–232.
- Chianelli, R.R., Ruppert, A.F., José-Yacamán, M., and Va'squez-Zavala, A. (1995) HREM studies of layered transition metal sulfide catalytic materials. *Catalysis Today*, 23, 269–281.
- Cornu, F. (1909) *Naturliches kolloides molybdänsulfid (Jordosit)*. Zeitschrift für Chemie und Industrie der Kolloide, 4, 190 (In German).
- Coveney, R.M., Jr. and Chen, N. (1991) Ni-Mo-PGE-Au-rich ores in Chinese black shales and speculations on possible analogues in the United States. *Mineralium Deposita*, 26, 83–88.
- Coveney, R.M., Jr. and Glascock, M.D. (1989) A review of the origins of metal-rich Pennsylvanian black shales, central U.S.A., with an inferred role for basinal brines. *Applied Geochemistry*, 4, 347–367.
- Coveney, R.M., Jr., Murowchick, J.B., Grauch, R.I., Chen, N., and Glascock, M.D. (1992) Field relations, origins and resource implications for platiniferous molybdenum-nickel ores in black shales, south China. *Exploration and Mining Geology*, 1, 21–28.
- Datye, A.K., Srinivasan, S., Allard, L.F., Peden, C.H.F., Brenner, J.R., Thompson, L.T. (1996) Oxide supported MoS₂ catalysts of unusual morphology. *Journal of Catalysis*, 158, 205–216.
- Disnar J.-R. (1981) Etude expérimentale de la fixation de métaux par un matériau sédimentaire actuel d'origine algale- II. Fixation 'in vitro' de UO₄²⁻, Cu²⁺, Ni²⁺, Zn²⁺, Pb²⁺, Co²⁺, Mn²⁺, ainsi que VO₅⁻, MoO₄²⁻ et GeO₃³⁻. *Geochimica et Cosmochimica Acta*, 45, 363–379.
- Dungey, K.E., Curtis, M.D., and Penner-Hahn, J.E. (1998a) Behavior of MoS₂ intercalation compounds in HDS catalysis. *Journal of Catalysis*, 175, 129–134.
- (1998b) Structural characterization and thermal stability of MoS₂ intercalation compounds. *Chemistry of Materials*, 10, 2152–2161.
- Fan, D. (1983) Polyelements in the lower Cambrian black shale series in southern China. In S.S. Augustithus, Ed., *Significance of trace metals in solving petrogenetic problems and controversies*, 447–474 p. Theophrastus Publications, Atens, Greece.
- Farragher, A.F. and Cossee, P. (1972) Catalytic chemistry of molybdenum and tungsten sulfides and related ternary compounds. In J.W. Hightower, Eds., *Proceedings, 5th International Congress on Catalysis*, 1301–1318.
- Gaines, R.V., Skinner, H., Catherine W., Foord, E.E., Mason, B., and Rosenzweig A. (1997) *Dana's New Mineralogy* (eighth edition). 1819 p. Wiley, New York.
- George, G.N., Kike, C.A., Prince, R.C., Sunde, R.A., Enemark, J.H., and Cramer, S.P. (1989) Structure of the active site of sulfite oxidase: X-ray absorption spectroscopy of the Mo(IV), Mo(V), and Mo(VI) oxidation States. *Biochemistry*, 28, 5075–5080.
- Glikson M., Chappell B.W., Freeman R.S., and Webber E. (1985) Trace elements in oil shales, their source and organic association with particular reference to Australian deposits. *Chemical Geology*, 53, 155–174.
- Golub, A.S., Shumilova, I.B., Novikov, Y.N., Mansot, J.L., and Danot, M. (1996) Phenanthroline intercalation into molybdenum disulfide. *Solid State Ionics*, 91, 307–314.
- Helz, G.R., Miller, C.V., Charnock, J.M., Mosselmans, J.F.W., Patrick, R.A.D., Garner, C.D., and Vaughan, D.J. (1996) Mechanism of molybdenum removal from the sea and its concentration in black shales: EXAFS evidence. *Geochimica et Cosmochimica Acta*, 60, 3631–3642.
- Kosidowski, L. and Powell, A.V. (1998) Naphthalene intercalation into molybdenum disulfide. *Journal of the Chemical Society, Chemical Communications*, 2201–2202.
- Leliveld, R.G., van Dillen, A.J., Geus, J.W., and Koningsberger, D.C. (1997) The sulfidation of γ -alumina and titania supported (cobalt) molybdenum oxide catalysts monitored by EXAFS. *Journal of Catalysis*, 171, 115–129.
- Lorimer G.W. and Cliff G. (1976) Analytical electron microscopy of minerals. In H.-R. Wenk, Eds., *Electron microscopy in mineralogy*, 564 p. Springer-Verlag, New York.
- Lott, D.A., Coveney, R.M., Jr., Murowchick, J.B., and Grauch R.I. (1999) Sedex nickel-molybdenum ores from south China. *Economic Geology*, 94, 1051–1065.
- Masuda H., O'Neil, J.R., Jiang, W.-T., and Peacor D.R. (1996) Relation between interlayer composition of authigenic smectite, mineral assemblages, I/S reaction rate and fluid composition in silicic ash of the Nankai Trough. *Clays and Clay Minerals*, 44, 443–459.
- Murowchick, J.B., Coveney, R.M., Jr., Grauch, R.I., Eldridge, C.S., and Shelton, K.L., (1994) Cyclic variations of sulfur isotopes in Cambrian stratabound Ni-Mo-(PGE-Au) ores of southern China. *Geochimica et Cosmochimica Acta*, 58, 1813–1823.
- Nissenbaum, A. and Swaine, D.J. (1976) Organic matter-metal interaction in recent sediments; the role of humic substances. *Geochimica et Cosmochimica Acta*, 40, 809–816.
- Payen, E., Kasztelan, S., Houssenbay, S., Szymanski, R., and Grimalt, J. (1989) Genesis and characterization by laser Raman spectroscopy and high-resolution electron microscopy of supported MoS₂ crystallites. *The Journal of Physical Chemistry*, 93, 6501–6506.
- Peacor, D.R., Coveney, R.M., Jr., and Zhao, G.M. (2000) Authigenic illite and organic matter—the principal hosts for vanadium in the Mecca Quarry Shale at Velpen, Indiana. *Clays and Clay Minerals*, 48, 311–316.
- Staples, L.W. (1951) Ilsemannite and jordisite. *American Mineralogist*, 36, 609–614.
- Stockmann, R.M., Zandbergen, H.W., Langeveld, A.D.V., and Mouljin, J.A. (1995) Investigation of MoS₂ on γ -Al₂O₃ by HREM with atomic resolution. *Journal of Molecular Catalysis A: Chemical*, 102, 147–161.
- Szilagyi, M. (1967) Sorption of molybdenum by humus preparations. *Geochemistry International*, 4, 1165–1167.
- Teo, B.K. (1986) EXAFS: basic principles and data analysis, 349 p. Springer-Verlag, Berlin.
- Topsøe, H., Clausen, B.S., and Massoth, F.E. (1996) Hydrotreating catalysis: science and technology. 310 p. Springer-Verlag, New York.
- Vissers, J.P.R., Scheffer, B., Beer, V.H.J.d., Mouljin, J.A., and Prins, R. (1987) Effect of the support on the structure of Mo-based hydrodesulfurization catalysts: activated carbon versus alumina. *Journal of Catalysis*, 105, 277–284.
- Volkov, I.I. and Formina, L.S. (1974) Influence of organic material and processes of sulfide formation on distribution of some trace elements in deep-water sediment of Black Sea. *AAPG Memoir*, 20, 457–476.

MANUSCRIPT RECEIVED JANUARY 31, 2000

MANUSCRIPT ACCEPTED FEBRUARY 7, 2001

MANUSCRIPT HANDLED BY ADRIAN J. BREARLEY